Towards large and powerful radio frequency driven negative ion sources for fusion

B. Heinemann, Ursel Fantz, W. Kraus, L. Schiesko, Christian Wimmer, Dirk Wünderlich, F. Bonomo, M. Fröschle, R. Nocentini, R. Riedl

Angaben zur Veröffentlichung / Publication details:

Heinemann, B., Ursel Fantz, W. Kraus, L. Schiesko, Christian Wimmer, Dirk Wünderlich, F. Bonomo, M. Fröschle, R. Nocentini, and R. Riedl. 2017. "Towards large and powerful radio frequency driven negative ion sources for fusion." *New Journal of Physics* 19 (1): 015001. https://doi.org/10.1088/1367-2630/aa520c.

New Journal of Physics
The open access journal at the forefront of physics

Deutsche Physikalische Gesellschaft DPG IOP Institute of Physics

PAPER • OPEN ACCESS

Towards large and powerful radio frequency driven negative ion sources for fusion

To cite this article: B Heinemann *et al* 2017 *New J. Phys.* **19** 015001

IOP Publishing New J. Phys. 19 (2017) 015001 doi:10.1088/1367-2630/aa520c

New Journal of Physics
The open access journal at the forefront of physics

Deutsche Physikalische Gesellschaft DPG
IOP Institute of Physics

Published in partnership with: Deutsche Physikalische Gesellschaft and the Institute of Physics

OPEN ACCESS

RECEIVED
27 September 2016

REVISED
29 November 2016

ACCEPTED FOR PUBLICATION
6 December 2016

PUBLISHED
6 January 2017

PAPER

Towards large and powerful radio frequency driven negative ion sources for fusion

B Heinemann[1], U Fantz, W Kraus, L Schiesko, C Wimmer, D Wünderlich, F Bonomo, M Fröschle, R Nocentini and R Riedl

Max-Planck-Institut für Plasmaphysik, Boltzmannstraße 2D-85748, Garching bei München, Germany
[1] Author to whom any correspondence should be addressed.

E-mail: bernd.heinemann@ipp.mpg.de

Keywords: neutral beam injection, negative ion source, radio frequency source, ITER, ELISE

Abstract

The ITER neutral beam system will be equipped with radio-frequency (RF) negative ion sources, based on the IPP Garching prototype source design. Up to 100 kW at 1 MHz is coupled to the RF driver, out of which the plasma expands into the main source chamber. Compared to arc driven sources, RF sources are maintenance free and without evaporation of tungsten. The modularity of the driver concept permits to supply large source volumes. The prototype source (one driver) demonstrated operation in hydrogen and deuterium up to one hour with ITER relevant parameters. The ELISE test facility is operating with a source of half the ITER size (four drivers) in order to validate the modular source concept and to gain early operational experience at ITER relevant dimensions. A large variety of diagnostics allows improving the understanding of the relevant physics and its link to the source performance. Most of the negative ions are produced on a caesiated surface by conversion of hydrogen atoms. Cs conditioning and distribution have been optimized in order to achieve high ion currents which are stable in time. A magnetic filter field is needed to reduce the electron temperature and co-extracted electron current. The influence of different field topologies and strengths on the source performance, plasma and beam properties is being investigated. The results achieved in short pulse operation are close to or even exceed the ITER requirements with respect to the extracted ion currents. However, the extracted negative ion current for long pulse operation (up to 1 h) is limited by the increase of the co-extracted electron current, especially in deuterium operation.

1. Introduction

Compared to filament based ion sources the radio frequency (RF) driven sources have the advantage of simplicity, reliability and longer lifetime.

In future large fusion machines RF sources are very attractive for the neutral beam systems, because of the in principle maintenance free operation. This is a very important advantage in a radioactive environment, where maintenance and repairs have to be carried out by remote handling. Moreover, the source wall material can be chosen freely, which offers more experimental flexibility to optimize the surface production of negative ions compared to filament sources, where the inner walls are coated with tungsten from the filaments during operation.

The target values of the accelerated ion current density are 230 A m^{-2} (H^-) and 200 A m^{-2} (D^-) respectively. The currents of the co-extracted electrons have to be smaller than that of the ions. Further requirements were operation in long pulses up to 3600 s (D^-) and 1000 s (H^-) at a maximum filling pressure of 0.3 Pa. The low pressure is necessary to keep the negative ion stripping losses in the extraction system low [1].

In 1996 IPP Garching started investigating the applicability of RF driven negative ion sources for the NBI of ITER [2]. The experiments were started with a small prototype source with 0.3 × 0.6 m^2 base area on the BATMAN and MANITU test facilities and is currently being continued with the large source of the ELISE test

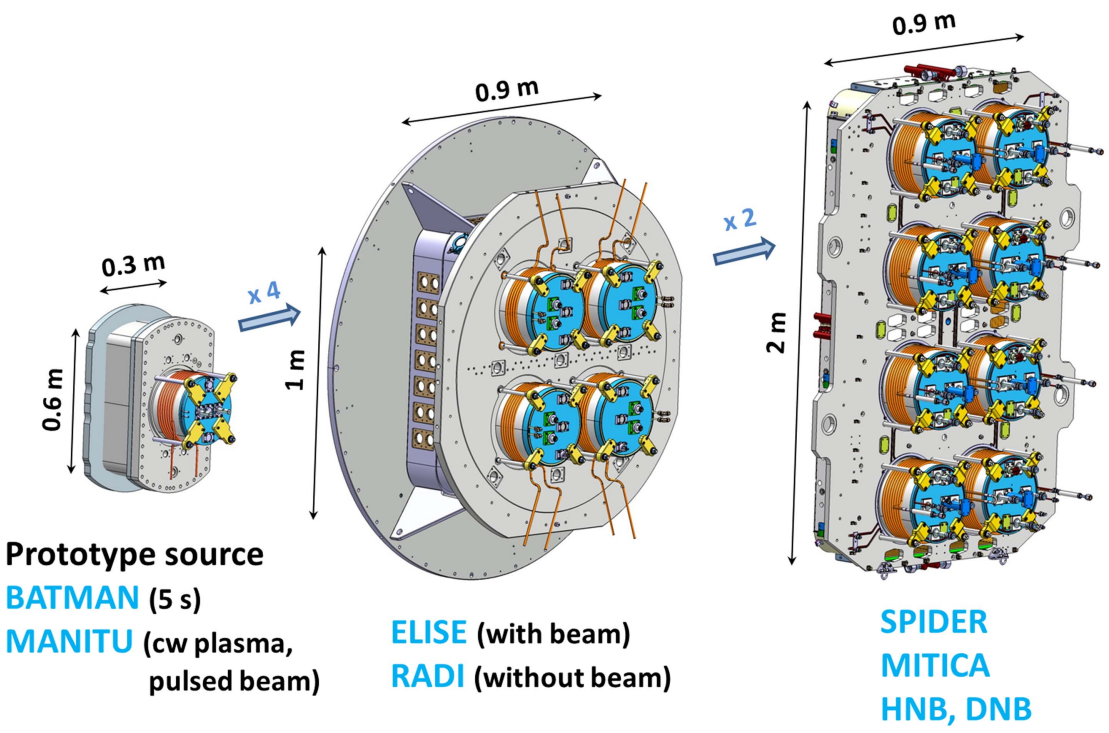

Figure 1. Modular concept of the RF source: from the prototype towards ion sources for ITER with ELISE as an intermediate step to prove the technological and physical concepts.

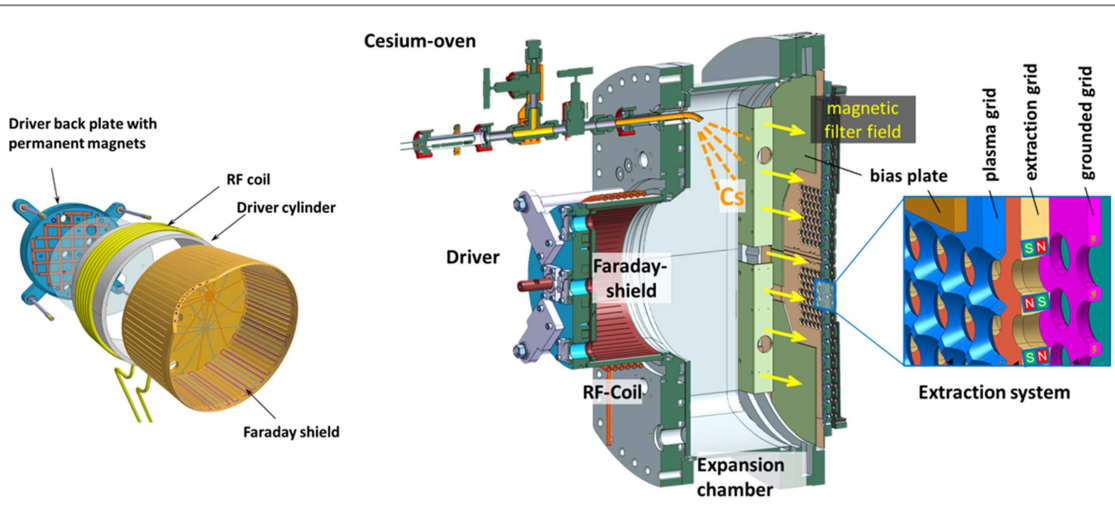

Figure 2. Schematic layout of the prototype source, left: exploded view of the driver, right: cross section through the ion source.

facility (0.9 × 1 m^2) which has half the size of the ITER source (0.9 × 2 m^2). ELISE is an intermediate step within the scientific roadmap to develop the ITER NBI source as shown in figure 1. The full size source will be used in the heating and diagnostic injectors (HNB and DNB) of ITER and first tested at the SPIDER and MITICA test facilities at RFX in Padua [3].

2. RF sources for negative neutral beam injection systems (NNBI)

2.1. Principle of RF sources for negative ion production

The operating principle of these RF sources is indicated in figure 2: the plasma is generated in the cylindrical source volume by inductive coupling of the RF power (up to 100 kW, $f = 1$ MHz) by an external coil. This so-called 'driver' consists of an Al_2O_3 or quartz cylinder with a RF coil of typically 6 turns wound around it. On the inside it is protected from plasma erosion by a Faraday shield with vertical slits allowing the penetration of the

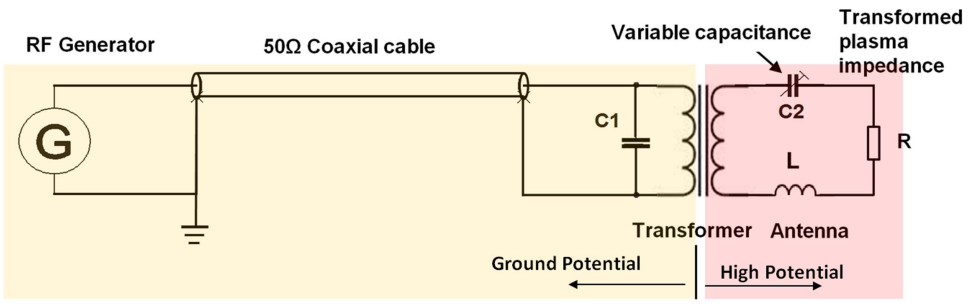

Figure 3. Matching circuit of the RF source.

magnetic RF-field. Because the Faraday shield prevents the capacitive coupling, a small starter filament is necessary to ignite the plasma. In sources with several drivers only one has to be equipped with a filament. Additionally the pressure is raised during the starting phase to ease plasma ignition.

The plasma expands out of the driver into the main source chamber. In order to avoid sputtering it is very important to coat the inner surfaces (made of copper for its thermal properties) by molybdenum, in particular surfaces exposed to high plasma density, like the Faraday shield. Otherwise the plasma grid can be covered by sputtered copper which would affect the negative ion production [4].

The main advantage of the driver concept is the modularity, which enables the extension to large sources by adding several drivers to one common expansion chamber.

Negative ions are predominantly produced via a surface conversion process of neutral atoms on the first grid (plasma grid, PG) close to the extraction apertures. This process can be enhanced significantly by evaporating caesium (Cs) into the source and depositing it on the plasma grid surface to reduce its work function. A magnetic filter field in front of the plasma grid is required to reduce the electron temperature in this region in order to minimize the destruction of negative ions by electron collisions and to reduce the amount of co-extracted electrons. The magnetic filter field is generated in the prototype source by rods of permanent magnets, which are mounted at 30 cm distance from each other along the sides of the plasma grid (see figure 2). They are installed in the diagnostic flange 3 cm upstream with respect to the PG or alternatively in an external magnet frame which can be shifted along the source axis in a range between 9 and 19 cm from the PG [5].

This field generation with permanent magnets is only possible in small ion sources, like the prototype source. In large sources like the ITER source, the width of 0.9 m exceeds by far the range of permanent magnets. In this case the filter field can be generated by a current of several kA flowing in vertical direction through the plasma grid (PG current). This solution is realized in the ELISE test facility, described in section 2.3.

A three grid extraction system is used in all test facilities to extract and accelerate the negative ions. The plasma grid (PG) has 80° chamfers on the plasma side to enhance the extraction probability for negative ions. The second grid, the extraction grid (EG), has further magnets embedded to deflect the co-extracted electrons out of the beam at low energies. They are deflected onto the surface of the EG which has a sophisticated cooling scheme integrated to scope with the high power load. The allowable power load on the EG is defining the maximum current of co-extracted electrons. The plasma is switched off to avoid thermal overloading of the EG if the product of measured electron current and extraction voltage exceeds the allowable limit (for ELISE the design value of acceptable power load is 200 kW per grid segment and plasma is switched off at 120 kW per segment for safety reasons).

The 'bias plate' (BP) is in principle an extension of the source walls, which covers the part of the plasma grid without extraction area and leads the source potential close to the extraction area. By applying a positive voltage to the plasma grid with respect to the bias plate the plasma in front of plasma grid can be influenced in a way that the current of co-extracted electrons is further reduced.

To control the Cs dynamics in the source, the plasma grid and bias plate is heated up to 200 °C and the inner walls of the main chamber are kept at elevated temperature of 35 °C–40 °C, the latter in order to avoid cold spots where Cs can be trapped.

For the power supply RF generators working at 1 MHz are used with powers up to 180 kW. As the generator is set on ground potential while the source is on high negative potential up to 60 kV, the RF power is transferred via a DC insulating ferrite core transformer. The matching circuit is shown in figure 3. Over many years the generators used were self-excited tube oscillators. Recently very promising experiments have been started with replacing them by transistorized amplifiers [6].

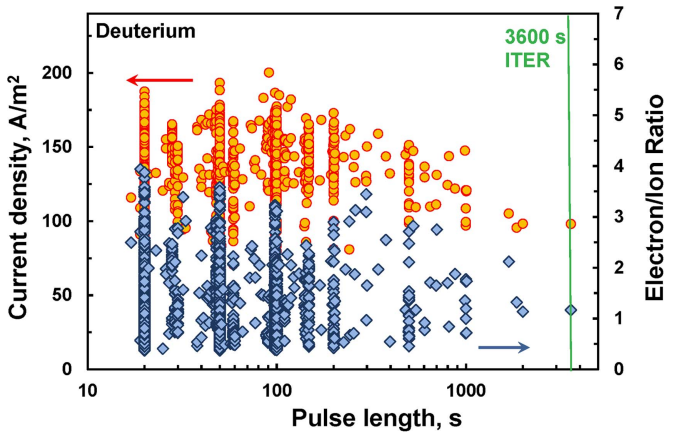

Figure 4. Source performance of MANITU for D^- operation in dependence of the pulse length.

2.2. Test facilities equipped with the prototype source: BATMAN and MANITU

On the test facilities BATMAN and MANITU the prototype source is used which has the size of roughly one eighth of the ITER source. The driver has a diameter of 24 cm and a volume of 7.7 l, the dimensions of the main chamber are $b \times l \times d = 31 \times 58 \times 23$ cm^3 (volume 40 l).

On the BATMAN test facility (BAvarian Test MAchine for Negative ions) the plasma pulse duration is limited to 7 s, beam extraction for maximum 5 s with up to 10 kV extraction and 15 kV acceleration voltage can be performed with an extraction area of 63.3 cm^2. The extraction system is derived from a positive ion extraction system using 126 apertures with a diameter of Ø 8 mm. This test facility is devoted to physical investigations and improvements of the source design and diagnostic systems [7].

At the MANITU test facility (Multi Ampere Negative Ion Test Unit) the prototype source and the test bed had been upgraded to enable a larger area beam extraction (approx. 200 cm^2) and long pulse operation up to 3600 s in H^- and D^-. The modifications to the source design for long pulses aimed at temperature control of all surfaces which are exposed to the plasma: actively cooling of the Faraday shield, which is the part with the highest power load, temperature control of the plasma grid by forced air flow and of the source side wall and back plate by tempered water. On this test facility stable long pulses in hydrogen and deuterium have been demonstrated. Figure 4 shows the extracted ion current densities and the electron to ion ratios in D^- operation achieved in one experimental campaign for all discharge parameters. Although the ion currents were limited in long pulses due to the increase of the electron current a maximum pulse length in deuterium of one hour has been achieved [8].

On both test facilities the required ITER parameters with respect to extracted current densities (329 A m^{-2} H^-, 289 A m^{-2} D^-), electron to ion ratio (<1), source pressure (0.3 Pa) and pulse length (1 h D^-, 400 s H^- at that time, meanwhile extended to 1000 s) could be achieved, but not simultaneously. Because of the positive results the RF source was selected in 2007 as the reference source for ITER.

MANITU has been shut down in 2011, because major components were needed for the ELISE test facility.

2.3. Test facilities RADI and ELISE

The extrapolation from the prototype source to ITER size sources is done in a modular way by using eight drivers attached to one expansion chamber. The challenges to be tackled for this step are the uniformity of plasma and extracted beam, the simultaneous operation of several drivers and the generation and topology of the filter field over the wide extraction area. For investigating these issues an intermediate step towards ITER was realized at IPP with two large RF sources which have the same source width but only half the height of the ITER source, the RADI and the ELISE sources. Both are equipped with four drivers supplied by two 180 kW/1 MHz RF generators. Each of the generators is connected to two neighboring drivers, which are connected in series.

The RADI source (inner dimensions: 0.76 × 0.8 m^2) had no beam extraction and was intended (i) to demonstrate the plasma uniformity of a RF source of ITER dimensions, (ii) to gain experience on operating several drivers simultaneously, pairwise connected in series, and (iii) to define operation parameters like gas flow, source pressure, etc [9]. Due to the small distance between the drivers of one pair, some mutual inductance exists which is suspected to have caused in the long run damages of the Faraday shields. Therefore the individual drivers were shielded on the outside by electromagnetic screens (EMS). Since then no further damage occurred. The RADI test facility is meanwhile shut down, because the RF generators were needed for the ELISE test facility.

ELISE is the next step involving beam extraction and including the technical experience gained at RADI: the base area of the ELISE source (extraction from a large ion source experiment) is slightly larger (0.87 × 1 m^2) in

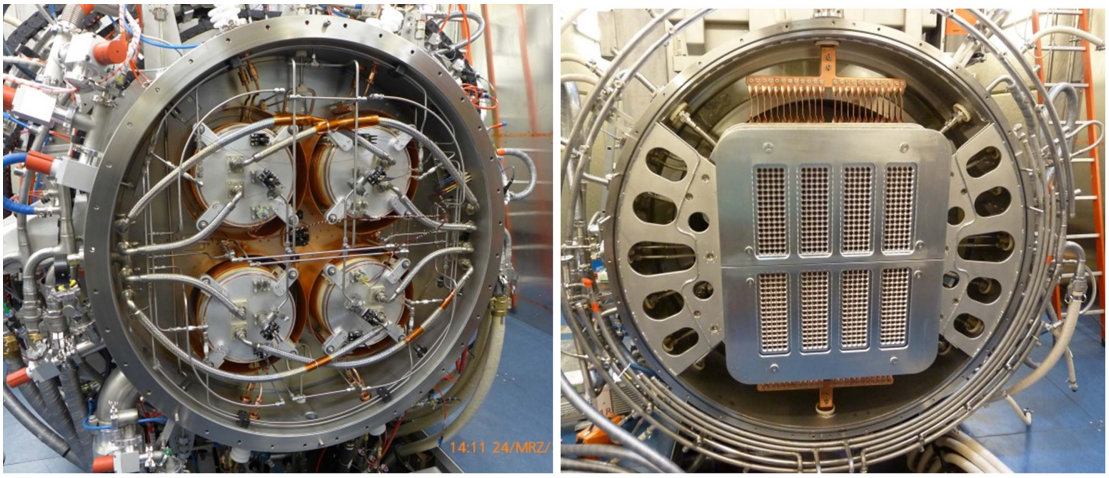

Figure 5. ELISE test facility, left: back side of ion source with 4 drivers (for operation in vacuum closed by a dome), right: view onto extraction system, showing the plasma grid and the bias plate; from the top the flexible copper conductors for the vertical PG current are visible, a corresponding connection is installed on the bottom side.

order to improve the plasma homogeneity at the edge of the extraction system [10]. Additionally the diameter of the drivers was increased from 24 cm (prototype and RADI) to 28 cm (ELISE) for better illumination of the extraction area by the plasma and a reduction of the power density in the drivers. A less pronounced neutral depletion effect [11] and a higher dissociation degree are also expected from this change due to the increased volume to surface ratio.

The design of the source and the extraction system follows as close as possible the ITER design. In order to have ITER like operation conditions the drivers are placed in vacuum. However, some modifications have been carried out to allow better diagnostic access and to improve the experimental flexibility. An overview is shown in figure 5 and presented in [12, 13].

The extraction system consists of three grids: plasma grid (PG), extraction grid (EG), grounded grid (GG) and a bias plate (BP) in front of the PG. Each grid has 640 apertures with a very similar aperture pattern (arranged in eight beamlet groups with 5 $\times$ 16 apertures each) and identical aperture geometry as ITER (Ø 14 mm), details are published in [12, 14, 15]. The grids are composed by two segments arranged on top of each other, a top and a bottom segment. For the EG and the GG these segments are electrically insulated against each other and against their grid support structure in order to measure individually the currents onto them.

Plasma operation of the source is possible up to 1 h, whereas beam extraction is pulsed with a duty cycle of 10 s/150 s due to limitations of the HV power supply. With an extraction area of 0.1 m^2 and beams of 60 kV/20 A ELISE is an important intermediate step towards the full size ITER source. Beam properties like uniformity, divergence and power are measured by several diagnostic tools. A detailed description of available source and beam diagnostics is given in section 3.

The magnetic filter field in ELISE is produced by a current up to 5.3 kA driven vertically through the PG. For a uniform field parallel to the extraction area a uniform current density distribution is achieved by a proper grid design [15]. Furthermore the three-dimensional topology of the field can strongly be influenced by the position of the return conductors of the PG current and is significantly different from that of the prototype source (see figure 6). In the prototype source only a week field penetrates into the driver but the uniformity across the extraction area is limited. On the contrary in ELISE the uniformity is very good, but a higher field penetrates into the drivers, although the return conductors are placed in the closest possible position beside the drivers. The experiments have shown that in ELISE a lower filter field is needed than expected: in hydrogen a field strength near the plasma grid of 2.2 mT and in deuterium of 3.2 mT is used. The values of the field integrated in the direction perpendicular to the PG are 0.4 mTm and 0.6 mTm respectively [16]. Corresponding numbers for the prototype source at BATMAN are 7 mT and 1–1.5 mTm for both species [5]. Increasing the filter field above these values reduces further the current of co-extracted electrons but also of the extracted negative ions. It is one of the main tasks of ELISE to study the filter field dependencies of the extracted current density, the co-extracted electron currents and the long pulse stability. Therefore a high flexibility of the position of the return conductors has been implemented in the source design; even crossing through the expansion volume is an option. The addition of external permanent magnets along the side walls of the source vessel which change the 3D topology of the filter field is also under investigation [17–19].

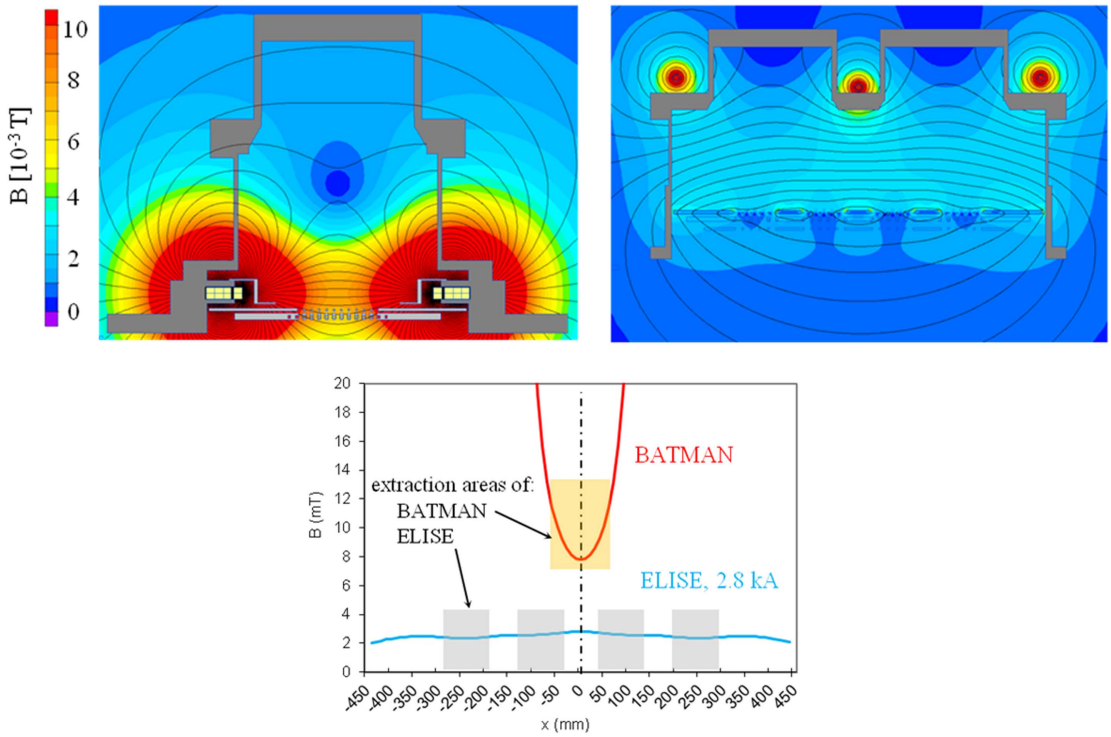

Figure 6. Comparison of the filter field of ELISE and the prototype source; top left: BATMAN in standard configuration with permanent magnets in the diagnostic flange, top right: ELISE with 2.8 kA PG current and return conductors beside drivers (standard configuration for H), bottom: profile of the total filter field across the PG for both cases.

For neutron shielding the entire test bed is encased in a concrete house, allowing beam extraction in deuterium up to 6 h a year.

ELISE is in operation since February 2013 and routine operation for short pulses (20 s plasma with 10 s beam) was demonstrated up to current densities of 256 A m^{-2} (H)/176 A m^{-2} (D). Also long pulses up 1 h (cw source plasma with 10 s beam blips every ≈150 s) could be performed at 0.3 Pa with limited RF power, achieving 153 A m^{-2} (H)/57 A m^{-2} (D). Further improvement of the source performance by increasing the RF power is limited so far by (i) RF break downs which occur randomly outside of the drivers and (ii) the amount and temporal stability of the co-extracted electron current, in particular in deuterium operation.

3. Diagnostic tools for the evaluation of source and beam performance

Diagnostic tools in the ion source and for the beam are required on the one hand in order to characterize the performance of the source and correlate it to the plasma parameters, on the other hand in order to understand the relevant physical processes, enabling the possibility for future optimization of the ion source. Although important parts of the source are not accessible for diagnostics (for example the boundary between the quasi-neutral source plasma and the extracted particle beam which is called meniscus), diagnostics are required in order to give input parameters and benchmark theoretical models describing individual parts of the ion source, including regions inaccessible to diagnostics [20]. Due to its flexible access for diagnostics mainly the BATMAN test facility is used at IPP for these kinds of benchmarks.

3.1. Source diagnostics

The expansion volume with the magnetic filter field divides the source plasma into two different regimes (typical plasma parameters determined by different diagnostics are listed in table 1):

In the driver, due to the elevated electron temperature and density an ionizing plasma is formed which is characterized by the dominance of inelastic electron collisions for the population of the individual excitation states [26] and its high dissociation degree of molecular hydrogen into atomic hydrogen [27]. Diagnostics in the driver need to withstand the elevated plasma density and electron temperature ($n_e = n_i \approx 10^{18}$ m^{-3}, $T_e \approx 10$ eV). For this reason, non-invasive diagnostics like the optical emission spectroscopy (OES) are preferable in this plasma regime.

Table 1. Typical plasma parameters in the driver and extended boundary layer of the RF source. Added in parenthesis are the diagnostics used for determination.

Parameter	Value in the driver	Value in the ext. boundary layer
Positive ion density n_{i^+}	$\approx 10^{18}$ m^{-3} (OES, [21])	$\approx 10^{17}$ m^{-3} (Langmuir probe, [22])
Electron density n_e	$\approx 10^{18}$ m^{-3} (OES, [21])	$< 10^{17}$ m^{-3} (Langmuir probe, [23])
H^- density n_{H^-}		$< 10^{17}$ (CRDS, [24])
Cs^0 density n_{Cs^0}	≈ 0 (OES)	$\approx 10^{15}$ m^{-3} (TDLAS, [25])
Electron temperature T_e	≈ 10 eV (OES, [21])	≈ 1 eV (Langmuir probe, [22]
Hydrogen density n_{H_2}	$\approx 10^{19}$ m^{-3} (pressure)	
Atomic fraction n_H / n_{H_2}	0.2–0.4 (OES, [21])	

Due to the reduced electron temperature and density ($n_e < n_i \approx 10^{17}$ m^{-3}, $T_e \approx 1$ eV), a recombining plasma is formed in the extended boundary layer close to the PG. In the recombining plasma, electron collisions are less important for the population of excited atomic or molecular states—in contrary, recombination processes are of high importance [26]. For this reason, emissivities measured by OES are much more complex to interpret. Invasive diagnostics as Langmuir probes become a useful tool for the determination of plasma parameters in this regime.

In the following, plasma and beam diagnostics used at the negative ion test facilities at IPP are discussed in more detail.

3.1.1. Optical emission spectroscopy

Using OES, the emissivity in the extended visible range (250–900 nm) of hydrogen Balmer lines (H), the molecular Fulcher band (H_2), caesium and impurities typically are determined. At the IPP test facilities, OES is used for three tasks:

- Detection of impurities as oxygen, nitrogen, the OH band or copper.
- Monitoring the stability of pulses by recording time traces of individual emission lines or bands.
- Quantitative evaluation for the determination of plasma parameters (mainly T_e, n_e, n_H / n_{H_2}, vibrational temperature T_{vib} and rotational temperature T_{rot}). For quantitative evaluation, the setup must be absolutely calibrated.

Depending on the task different measurement systems are used:

- Simple photo diodes with an interference filter for monitoring the plasma stability, e.g. the H_α radiation in the driver(s).
- Survey spectrometers (typical wavelength resolution of several 100 pm/pixel) for all tasks, including some quantitative evaluation (T_e, n_e, n_H / n_{H_2}). Figure 7(a) shows a typical spectrum in the extended boundary layer at BATMAN. The temporal evolution of the Balmer lines and Fulcher band during this BATMAN pulse is plotted in figure 7(b). An influence of the applied high voltage during the extraction phase is seen in the measured emissivities in the extended boundary layer.
- High resolution spectrometers (typical wavelength resolution in the order of 10 pm/pixel) for a more detailed detection of impurities (yielding a much better insight into the structure of the emission line or band) as well as for quantitative evaluation—in particular of the molecular Fulcher band for the determination of T_{vib} and T_{rot} [27].

For the determination of plasma parameters collisional radiative models describing the population and depopulation of the individual states for atomic and molecular hydrogen are applied [28, 29]. The application of such models is straight forward in the ionizing driver plasma; however, it is much more complex in the recombining plasma regime close to the PG, where many different channels (e.g. recombination processes and mutual neutralization of negative ions with positive ions) lead to the population of the individual excited states.

3.1.2. Langmuir probes

Langmuir probes are used in the extended boundary layer for determining the plasma parameters n_i, n_e, T_e, the floating potential Φ_{fl} and plasma potential Φ_{pl}. Movable probes allow for the determination of profiles (either in axial direction from the driver exit to the PG [30] or in horizontal and vertical direction in the extended boundary layer [23]), whereas fixed probes are used as a standard diagnostic for determining changes in the

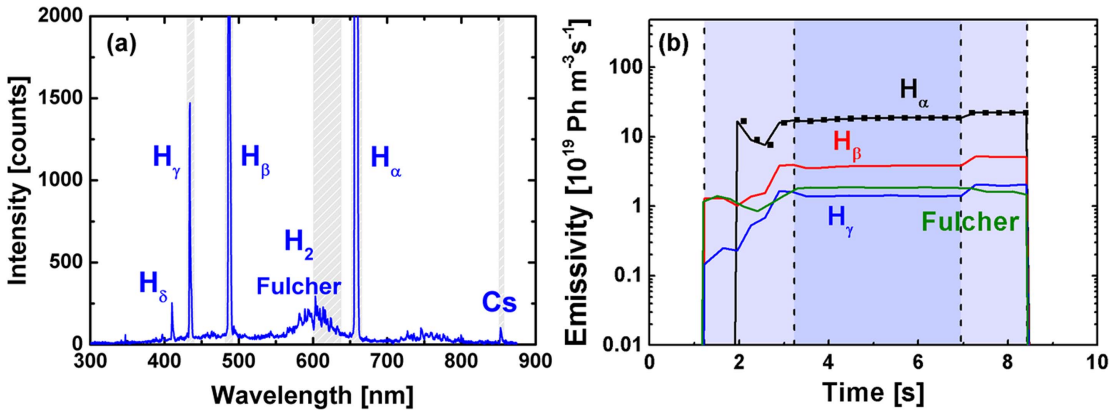

Figure 7. (a) Survey spectrum during a BATMAN pulse measured in the extended boundary layer. Marked in gray are the individual integration ranges. (b) Time traces of the H_α, H_β, H_γ and Fulcher emissivities during a BATMAN discharge in the extended boundary layer. H_α is overexposed during the beginning of the discharge. Marked in light blue is the time, during which RF is applied to the source; dark blue indicates the beam extraction phase.

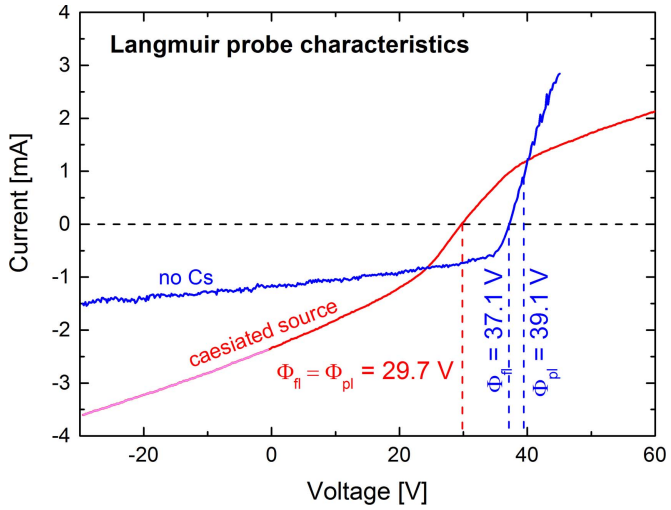

Figure 8. Langmuir probe characteristics in the extended boundary layer before Cs evaporation and in a well caesiated source, measured at BATMAN.

plasma parameters or the plasma asymmetry by using two probes. An axial profile of plasma parameters in the expansion chamber will be shown in figure 18(a). A sufficient plasma overlap in front of the PG from the four drivers has been demonstrated by laterally moveable probes at RADI [31]. Due to the oscillating plasma potential caused by the RF plasma generation as well as the magnetized electrons in the filter field, Langmuir probes require either RF compensation or a careful analysis of the positive ion branch of the *I–V* curve only, as well as a suitable probe tip radius with respect to the electron gyration radius and local Debye length.

Langmuir probes are the only diagnostics revealing information on the potentials in the plasma. In particular the plasma potential in the vicinity of the PG is of high interest, since the potential difference to the positively biased PG strongly influences the dynamics of charged particle fluxes onto and from the PG (mainly electrons from the plasma onto the PG as well as surface produced H^- from the PG into the plasma) and thus strongly influences the amount of extracted H^- and co-extracted electron current.

A clear transition of the plasma regime close to the PG takes place during the Cs conditioning process of the ion source: figure 8 shows two Langmuir probe characteristics recorded at BATMAN at an axial distance of 7 mm from the PG, one in a cleaned source before evaporating Cs (volume operation) and a second one in a well caesiated source. The classical Langmuir probe characteristics indicates an electron-ion plasma close to the PG in volume operation whereas the transition to a symmetric curve indicates the formation of an ion–ion plasma, in which negative hydrogen ions form the dominant negative charge flux to the Langmuir probe. During the caesiation of the source, also the plasma potential is significantly lowered (from 39.1 to 29.7 V), which is

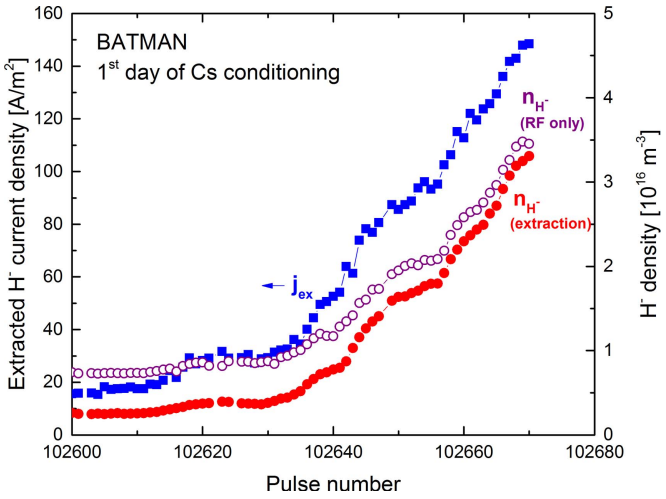

Figure 9. Extracted negative ion current density and H^- density during extraction (filled circles) and during RF only phase (open circles) for the first day of Cs conditioning of a BATMAN campaign. Operational parameters have been kept constant (0.3 Pa filling pressure, 60 kW RF power, 5 kV extraction voltage).

explained by a significant flux of surface-produced negatively charged particles from the walls into the plasma [32].

3.1.3. Cavity ring-down spectroscopy (CRDS)

CRDS is a sensitive absorption technique for the determination of the line-of-sight (LOS) integrated H^- density [24]. CRDS is based on the photo detachment process of H^-: $H^- + h\nu \rightarrow H + e^-$. Due to the low cross-section of this process (3.5×10^{-21} m^2 at a wavelength of 1064 nm [33]), classical absorption techniques suffer from sensitivity. For this reason, CRDS uses a high finesse optical cavity formed by two mirrors ($R > 99.99\%$), which is excited by a ns-scale laser pulse. The LOS integrated H^- density can be calculated by the comparison of the decay time of the empty cavity with the decay time during the plasma pulse, the latter including H^- as an additional absorber. At BATMAN, a negative hydrogen ion density in the order of 10^{16} m^{-3} is measured during pure volume operation; this density is increased by up to one order of magnitude during caesiation of the source [24, 32].

Plotted in figure 9 is the evolution of the extracted negative hydrogen ion density as well as the H^- density during extraction and during RF only phase in front of the plasma grid (axial distance of 2.2 cm) for the first day of Cs conditioning at BATMAN. In general, the H^- density in the plasma volume shows the same trend as the extracted negative ion current density. The effect of the extraction on the H^- density (comparison between extraction and RF only phases) becomes less pronounced when the source is better conditioned. The transport of negative ions changes drastically during the shown first conditioning from negative ions solely produced in the plasma volume (clean source without Cs) towards surface production, where negative ions predominately origin from the caesiated surfaces.

3.1.4. Tunable diode laser absorption spectroscopy (TDLAS)

TDLAS is applied at BATMAN for the determination of the LOS integrated neutral Cs density n_{Cs^0} [34]. TDLAS uses a single-mode diode laser, whose wavelength is tuned over the Cs 852 nm resonance line for recording an absorption spectrum. In contrast to OES, TDLAS determines the neutral Cs density without the requirement of any knowledge of plasma parameters in plasma phases and additionally in vacuum phases of the pulsed-driven test facilities. The vertical Cs symmetry can be determined by using two horizontal LOS (the vertical Cs symmetry is of importance since in the standard setup of BATMAN only one Cs oven is mounted in the top part of the source [25]). These features make TDLAS an important diagnostics for gaining insight into the complex Cs dynamics in the ion source. The typical neutral Cs density during plasma phases at BATMAN is in the order of 10^{15} m^{-3}, in vacuum phases it can be up to one order of magnitude lower, the latter strongly depending on the Cs evaporation rate of the oven [25].

The neutral Cs density measured in the top and bottom part of the source for two pulses during an operational day at BATMAN is shown in figure 10. The Cs density in the vacuum phase before and after the plotted seventh pulse of the day is below the detection limit ($<10^{14}$ m^{-3}). In case of the 130th pulse of the day, the neutral Cs density in the vacuum phase before and after the pulse is roughly two times higher at the top LOS than at the bottom LOS, caused by the fact that the Cs oven is mounted in the top part of the back plate of the

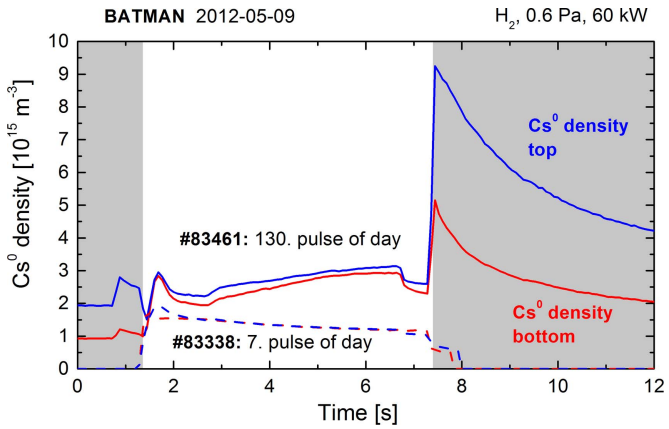

Figure 10. Neutral Cs density in the top and bottom part of the source for the seventh and 130th pulse of an operational day at BATMAN.

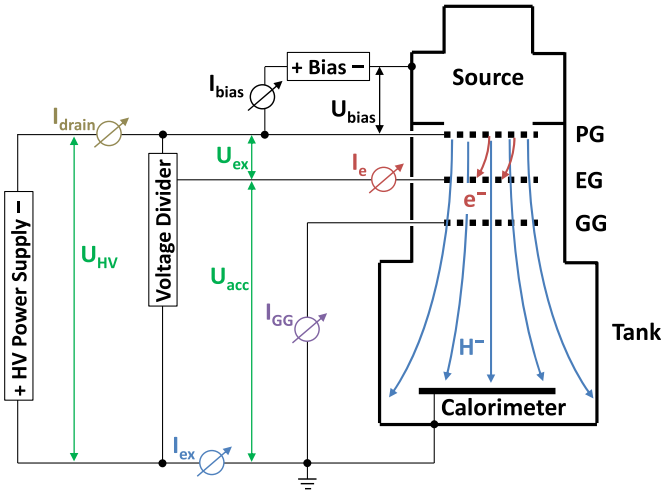

Figure 11. Schematic view of the high voltage circuit of the prototype source, including the bias circuit of the PG.

expansion chamber. For both pulses during the plasma phase, a similar neutral Cs density is detected at both lines of sight (10^{15} m^{-3} for the seventh pulse and 2–3 $\times$ 10^{15} m^{-3} for the 130th pulse). The temporary increase of the neutral Cs density in the vacuum phase after the pulses is explained by the lack of ionization processes after turning off the RF plasma heating. The density decreases afterward back to equilibrium within several seconds. Due to redistribution processes in the plasma, Cs is distributed almost homogeneously during the plasma phases of both shown pulses. A more detailed explanation of the Cs dynamics at BATMAN can be found in [25].

3.2. Beam diagnostics

3.2.1. Electrical current measurements

In order to gain a global view of the source performance, the extracted electrical negative ion current I_{ex} (total current to ground, i.e. on tank, calorimeter and grounded grid), electron current I_e (current on extraction grid) and the current on the grounded grid I_{GG} are measured in all beam test facilities. In addition, the total current to the high voltage power supplies I_{drain} is measured (which must be equal to the sum of I_{ex} and I_e). The high voltage circuit of the prototype source is illustrated in figure 11 including the positive bias of the PG with respect to the source body. The HV layout is similar for the ELISE test facility [35] with the exception of the vertical division of the extraction and grounded grid in two segments, allowing in particular for determination of the individual co-extracted electron currents in the upper and the lower half of the extraction system. Thus, possible asymmetries in the co-extracted electron current can be identified.

The evolution of the extracted negative ion and co-extracted electron current density during the first day of Cs conditioning at the BATMAN test facility is shown in figure 12. The extracted H^- current density is increased by a factor of 9.7 while j_e is decreased by a factor of 1.8 during this operational day. The achieved ratio of

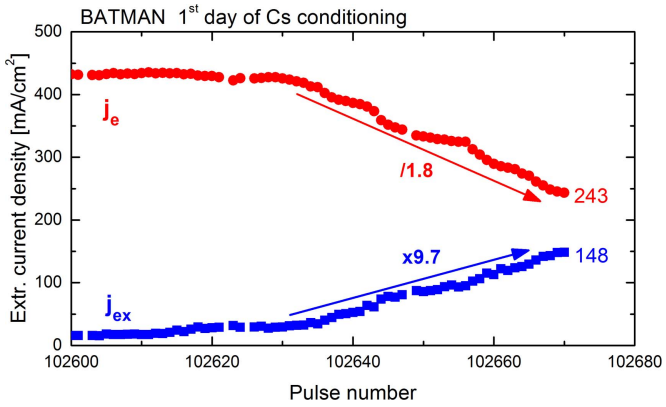

Figure 12. Evolution of the extracted H^- current density and the co-extracted electron current density during the first day of Cs conditioning of a BATMAN campaign. Operational parameters have been kept constant (0.3 Pa filling pressure, 60 kW RF power, 5 kV extraction voltage).

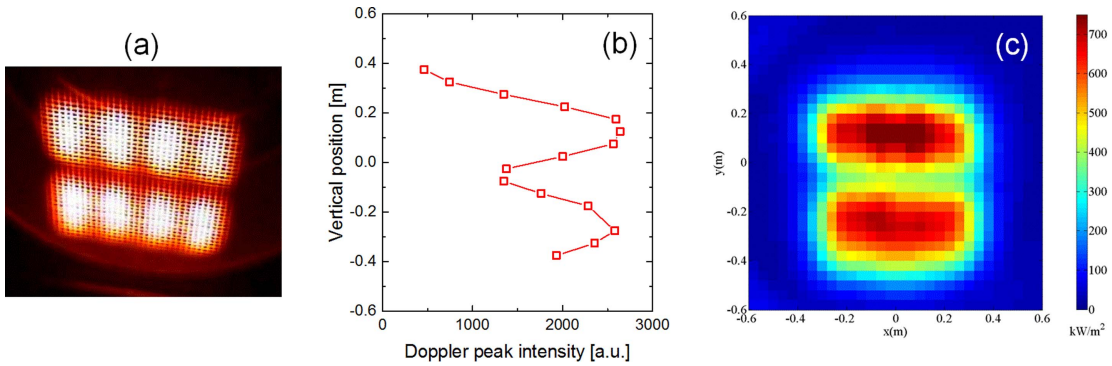

Figure 13. (a) Beam pattern on the tungsten wire calorimeter during an ELISE beam pulse. (b) Vertical beam profile determined by BES for the same pulse. (c) IR image of the diagnostic calorimeter for the same pulse. Discharge parameters: hydrogen, RF power 31 kW/driver, UHV = 30 kV, $j_{ex} = 123$ A m^{-2}.

$j_e/j_{ex} = 1.6$ at the end of this day indicates that the source is not yet in good Cs condition; in good condition a value for j_e/j_{ex} way below 1 can be reached in hydrogen operation.

3.2.2. Tungsten wire calorimeter

In order to get a rough shape of the beam extracted at ELISE and BATMAN as well as for a rough estimation of the beam divergence, the beam intersects a tungsten wire calorimeter, a grid of tungsten wires [36]. The thickness of the tungsten wires (200–300 μm) has been chosen so that the temperature increase for typical beam parameters is up to 2600 K (thermal equilibrium reached in about 1 s). A CCD camera (visible light) records a video of the tungsten wires. An image of the tungsten wire calorimeter during beam extraction at ELISE is shown in figure 13(a). The individual tungsten wires are spaced by 20 mm, the calorimeter is mounted 1.8 m downstream of the grounded grid. The eight individual beamlet groups of ELISE are clearly distinguishable, as long as good beam optics is chosen.

3.2.3. Beam emission spectroscopy (BES)

BES is based on the measurement of Doppler-shifted H_α radiation emitted from excited hydrogen atoms created by collision of the beam with background gas particles. For this purpose, lines of sight with a certain angle to the beam direction are used. BES yields information about three quantities: the intensity of the fully accelerated beam (which is proportional to the integral over the fully Doppler-shifted peak), the beam divergence (correlating with the FWHM of the fully Doppler-shifted peak) as well as the amount of H^- ions stripped in the accelerator (leading to a non-fully Doppler-shifted peak). At BATMAN, 5 horizontal LOS with a vertical spacing of 40 mm are installed, allowing the determination of a vertical beam profile. ELISE is equipped with 16 horizontal LOS with a spacing of 50 mm and 4 vertical LOS with a spacing of 160 mm [36], the lines of sight intersect the beam at an axial distance of roughly 2.6 m from the grounded grid. A typical vertical beam

profile at ELISE (integral of the fully Doppler-shifted peak) is shown in figure 13(b). The upper and lower beamlet groups are clearly divided.

3.2.4. Diagnostic calorimeter

The diagnostic calorimeter acts as a beam dump at each beam test facility. The most sophisticated diagnostic calorimeter is installed at ELISE [36]: a pattern of 30 × 30 copper blocks (surface of 38 mm × 38 mm, spacing of 2 mm, thickness of 25 mm) is mounted on a back plate; the latter incorporates a water cooling circuit. Thermocouples are embedded in 48 blocks. The diagnostic calorimeter is mounted 3.5 m downstream the grounded grid. Three diagnostics are using this calorimeter:

- By means of calorimetric measurement of the cooling water the global beam power is calculated (available at all beam test facilities; at ELISE measured separately in four quadrants).
- The embedded thermocouples provide a shape of the beam profile as well as the beam power (available at all beam test facilities; at BATMAN 29 thermocouples are used).
- An IR camera measures the temperature increase of the individual blocks (only available at ELISE) allowing for thermography. Both, beam profile and power can be determined.

An image of the IR camera during beam extraction at ELISE is shown in figure 13(c). The individual copper blocks lead to a pixelated structure of the image. The top and bottom beamlet groups are clearly divided. Due to the longer distance from the grounded grid in comparison to the tungsten wire calorimeter, the four horizontal beamlet groups are strongly overlapping on the diagnostic calorimeter.

4. Comparison of hydrogen and deuterium operation

For identical source parameters (RF power, filling pressure, extraction voltage, etc…) and magnetic field configuration, the absolute value and the temporal stability of the extracted negative ion current and the co-extracted electron current for ion source operation in deuterium can significantly differ from results in hydrogen operation. This behavior is correlated to differences in the plasma structure and the plasma parameters, for example the positive ion density and the plasma potential. This section highlights and discusses the properties of hydrogen and deuterium plasmas as well as the beam.

4.1. Performance in H_2 and D_2

Figure 14 shows the source performance for short pulses (7.2 s plasma phase, 4.5 s beam extraction) at BATMAN in hydrogen (upper part of the figure) and deuterium (lower part of the figure) at $p_{\mathrm{fill}} = 0.6$ Pa and using the filter field created by magnets in the external frame. Shown are results of pulses performed for different values of the extraction potential, the bias potential, the RF power and different status of the caesium conditioning. For each pulse one value (averaged over the second half of the beam extraction) is presented.

The maximum achievable extracted negative ion current density in deuterium is comparable with the results in hydrogen but the amount of co-extracted electrons, however, is generally much larger. Due to the limit of the power deposited by the electrons onto the EG this effect can strongly restrict the source performance obtainable in deuterium operation.

For hydrogen and $j_{\mathrm{ex}} < 300$ A m^{-2} the electron-ion-ratio remains roughly constant with increasing P_{RF}. In contrast for deuterium the electron-ion-ratio increases with P_{RF}. This behavior is in general agreement with results obtained at ELISE [19].

Figure 15 demonstrates the isotope effect in the temporal behavior of the performance during single pulses. Shown are the extracted negative ion current densities and the electron-ion-ratio for pulses in ELISE at 0.3 Pa. Figure 15(a) illustrates results for short pulses (20 s plasma phase, 9.5 s beam extraction), figure 15(b) for long pulses (3600 s plasma pulse, 20 × 9.5 s pulsed beam extraction, one averaged value per beam extraction phase). The best pulses up to now have been chosen, i.e. pulses combining j_{ex} as high as possible together with $j_{\mathrm{e}}/j_{\mathrm{ex}} < 1$. Shown in the top part of figure 15 are results for hydrogen, in the bottom part results for deuterium.

The same amount of RF power was injected for both isotopes (short pulses: 50 kW/driver, long pulses: 20 kW/driver). Due to the higher amount of co-extracted electrons, in deuterium a lower extraction potential, a higher bias potential and a higher magnetic filter strength have been used.

For *short pulses* (figure 15(a)) the extracted negative ion currents are stable, both in hydrogen and deuterium. In contrast, the electron-ion-ratio in deuterium starts at a much higher value than in hydrogen and it increases much faster during the course of the pulses. This effect is a general one that is observed at all test facilities [37].

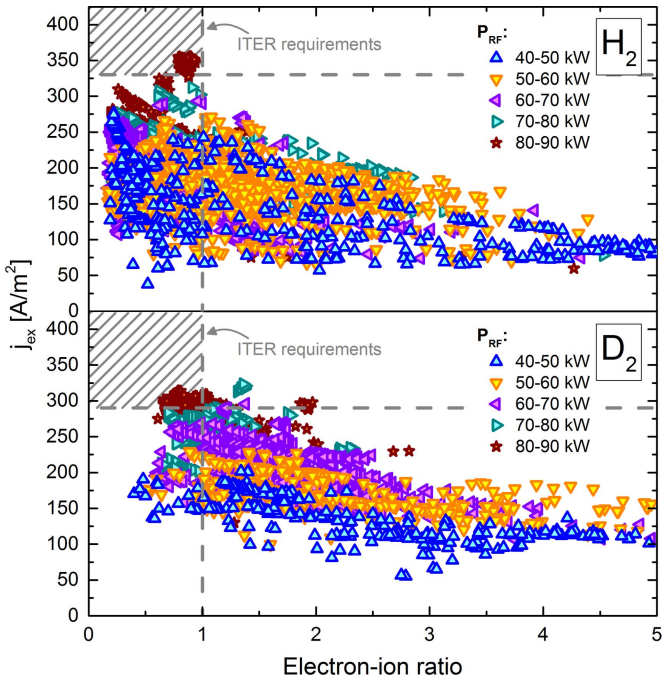

Figure 14. Comparison of the performance obtained at BATMAN in hydrogen and deuterium for different values of the RF power at $p_{fill} = 0.6$ Pa.

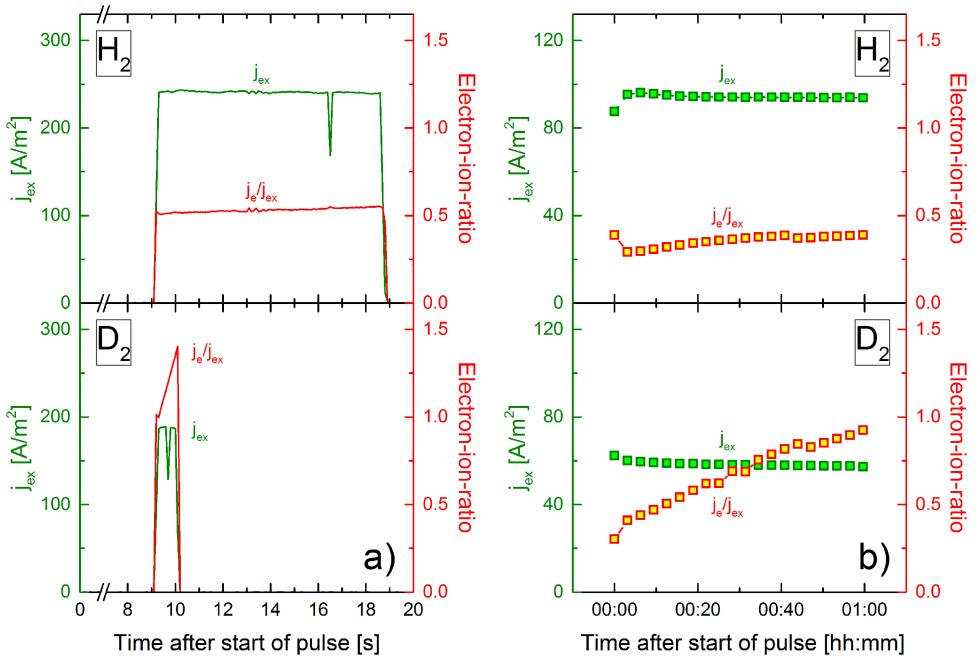

Figure 15. Time traces of the extracted ion current (green) and the electron-ion-ratio (red) at ELISE in hydrogen and deuterium operation and $p_{fill} = 0.3$ Pa. (a) short pulses; (b) one hour plasma pulses with 20 beam blips.

Due to this strong increase of the co-extracted electrons the deuterium pulse is stopped prematurely (after around 1 s) to avoid thermal overloading of the EG.

Long pulse operation was possible up to 1 h, even in deuterium (figure 15(b)) but at reduced source parameters. The starting value of the electron-ion-ratio for deuterium operation is comparable to hydrogen operation. This result seems to be in contradiction to the statement that j_e/j_{ex} generally is higher in deuterium but it can be explained by the different source parameters used for the two isotopes. During the 1 h pulse in hydrogen a distinct improvement of the source performance can be seen between the first and the second beam blip. Reason is that this pulse has been performed at the beginning of the respective operating day, i.e. it was not

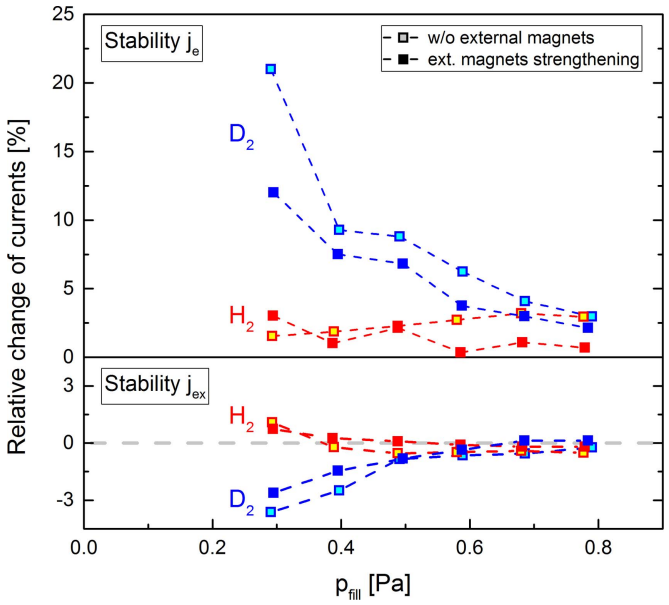

Figure 16. Stability of the extracted negative hydrogen current density and the co-extracted electron current in ELISE during short pulses in hydrogen and deuterium, with and without the strengthening external magnets.

preceded by the usually performed daily caesium conditioning process. Instead, the caesium conditioning took place during the first minutes of the long plasma pulse. For both isotopes the electron-ion-ratio increased during the pulse but this increase is much more pronounced in deuterium [19].

In order to investigate the dependence of the temporal behavior of the extracted currents on the source parameters, dedicated short pulse experiments have been performed at ELISE with the following source parameters: $P_{RF} = 20$ kW/driver, $p_{fill} = 0.6$ Pa, $I_{Bias} = 55$ A. Different values for the extraction potential (hydrogen: 4 kV, deuterium: 3 kV) and the PG current (defining the strength of the magnetic filter; hydrogen: 2.5 kA, deuterium: 4 kA) have been used for the two isotopes. Figure 16 shows for both isotopes the temporal change during the pulse (in percent) of the extracted negative ion current j_{ex} and the electron-ion-ratio versus the filling pressure. Open symbols show results for the magnetic filter generated only by the current I_{PG} while full symbols represent measurements with external magnets attached to the side walls strengthening the I_{PG} field [17–19].

For hydrogen operation the co-extracted electron current increases only slightly during the 9.5 s beam extraction phase. The magnitude of this increase does not depend on the filling pressure. The extracted negative ion current is stable for all investigated values of the pressure. These results are valid without and with the strengthening external magnets.

In deuterium the temporal behavior of both ion and co-extracted electron current depend on the filling pressure: while for $p_{fill} \geqslant 0.7$ Pa the results are comparable to hydrogen, for decreasing the pressure toward ITER values ($\leqslant$0.3 Pa) a much stronger increase of j_e during the pulses is observed, accompanied by a slight decrease of j_{ex}. This decrease of j_{ex} with increasing j_e can be explained by an increasing electron density in the plasma volume close to the extraction apertures, resulting in an increased negative space charge generated by these electrons and additionally an increased probability for destruction of negative ions by electron collision.

Using the additional external magnets, the increase of the co-extracted electrons in deuterium at $p_{fill} = 0.3$ Pa is reduced by more than 40%. The external magnets additionally result in a significant reduction of the absolute amount of co-extracted electrons and only a slight reduction of the extracted negative ions (see figure 23). These magnets were a prerequisite for performing at ELISE plasma pulses over one hour in deuterium at 0.3 Pa.

Up to now, no full explanation for the observed strong differences between the results obtained in hydrogen and deuterium operation is known. The main physical property in which hydrogen differs from deuterium is its mass. This may have an influence on reaction probabilities, e.g. for interaction with the caesium reservoirs in the ion source. Additionally and as a consequence of the mass difference the energy eigenvalues for the molecular vibrational and rotational sub-states and the population distribution of these states differ.

In order to improve the understanding of the physics behind the observed isotope effect, several diagnostic techniques have been applied in order to systematically measure the parameters in the plasma and the beam for both isotopes.

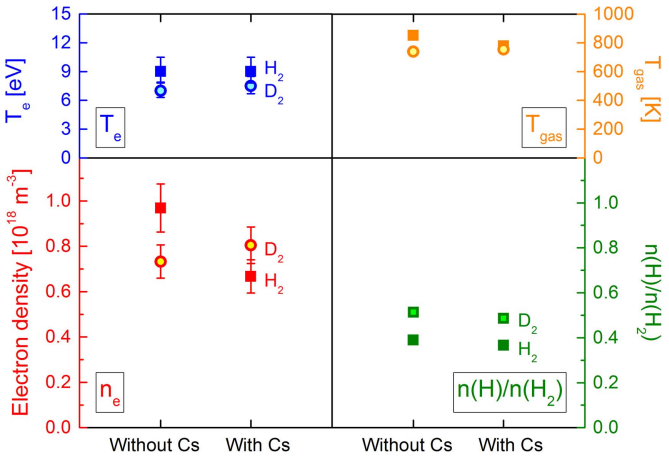

Figure 17. Plasma parameters obtained by OES for the driver of BATMAN in hydrogen and deuterium operation with and without caesium at $p_{\text{fill}} = 0.6$ Pa.

4.2. Plasma parameters in H_2 and D_2

Shown in figure 17 are results of OES measurements performed in the driver of BATMAN [21]. In this ionizing plasma, hydrogen molecules are dissociated into hydrogen atoms. The hydrogen atoms are then converted into negative ions by impinging on the low work function PG surface. Full symbols represent results for hydrogen, open ones deuterium. The measurements have been performed at $p_{\text{fill}} = 0.6$ Pa, $P_{\text{RF}} = 70$ kW, using the filter field created by magnets in the external frame and with and without caesium present in the ion source volume.

The electron temperature is slightly lower in deuterium. Taking into account the large error bars and the non-systematic behavior of the results, no clear statement can be made regarding the isotope dependence of the electron density. The gas temperature does not depend on the isotope. The vibrational temperature in the molecular ground state (not shown here) was determined for both isotopes to 5000 K. The only clearly observable isotope effect is in the atomic to molecular density ratio: the dissociation is higher in deuterium than in hydrogen. The higher dissociation in deuterium at almost the same plasma parameters is most probably a result of the dissociation cross sections that are higher for deuterium than for hydrogen [38]. At 8 eV roughly a factor of two is obtained between the cross sections for dissociation of the lowest vibrational level $v = 0$ in the molecular ground state, decreasing slightly with increasing vibrational quantum number.

The influence of adding caesium on the plasma parameters in the driver is small. A much stronger influence is observed in the plasma region close to the PG where, as shown in figure 9, the negative hydrogen ion density significantly increases when caesium is added. The simultaneous decrease of the electron density with caesium can be observed by Langmuir probes measurements (see for example figure 8).

The observed trends are in agreement with previous measurements performed at BATMAN with the standard configuration of the magnets, i.e. inside the source [27].

Movable Langmuir probes in BATMAN [39] allow investigating the expansion of the plasma from the driver towards the PG and how this expansion depends on the isotope: figure 18(a) shows, for hydrogen and deuterium, the positive ion density measured in the upper and the lower part of the ion source (at $p_{\text{fill}} = 0.6$ Pa, $U_{\text{ex}} = 5$ kV, $U_{\text{acc}} = 10$ kV and with the embedded filter magnets). The positive ion density shows for both probe positions a pronounced profile with a local maximum in 5–12 cm distance from the PG. Similar profiles have also been observed for the filter field generated by the external frame [39]. The general shape of the profiles is comparable for H_2 and D_2; the local maxima are shifted slightly toward the PG for deuterium. The reason for these profiles is a complex interplay of different drift effects. Density profiles calculated using a 2D fluid code with a planar symmetry [40] are in good general agreement with the Langmuir probe results, as can be seen in figure 18(b), showing the calculated 2D profile [41] of the electron density. The magnetic filter causes a strong decrease of the electron temperature close to the PG. Due to the interplay of diamagnetic drifts and $E \times B$ drifts local minima of the electron temperature are formed that are accompanied by the local maxima of the plasma density observed by the probes.

Close to the PG the plasma density measured by the Langmuir probes is higher in the upper part of the plasma. The plasma in this region is more homogeneous for operation in deuterium. These results are in agreement with results of other diagnostics, e.g. OES [42].

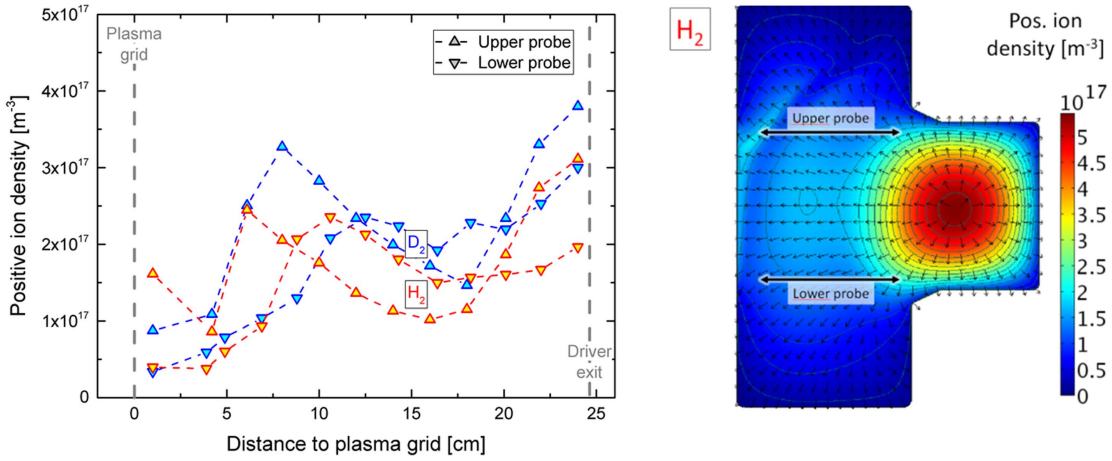

Figure 18. (a) Axial profiles of the positive ion density in BATMAN measured using two movable Langmuir probes located in the top part and the bottom part of the expansion region ($p_{fill} = 0.6$ Pa). Red: hydrogen; blue: deuterium. (b) 2D profile of the positive ion density calculated using a 2D fluid code [40, 41]. The arrows indicate the positive ion flux.

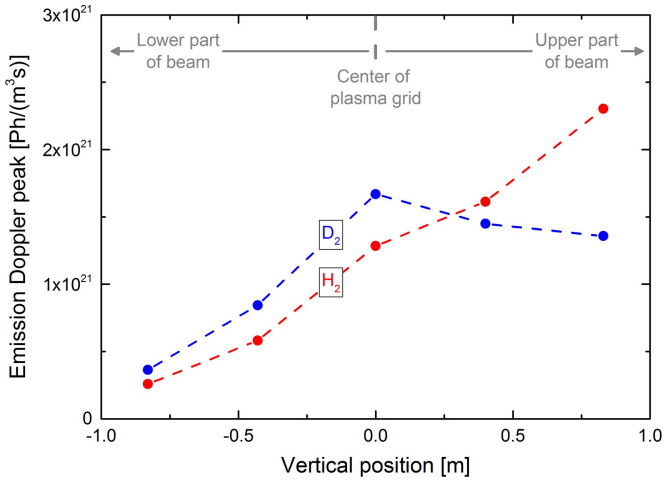

Figure 19. Vertical profiles of the beam measured at BATMAN (using beam emission spectroscopy) for hydrogen and deuterium discharges.

4.3. Beam properties in H_2 and D_2

BES measurements of the beam have been carried out in order to correlate the plasma properties to the beam properties. Figure 19 shows an example of BATMAN at 0.3 Pa, using the embedded filter magnets, $U_{ex} = 5$ kV and $U_{acc} = 15$ kV. Plotted is a profile of the beam intensity deduced from the integrated emissivity of the fully shifted Doppler peak measured along the five BES lines of sight.

For both isotopes approximately the same negative ion current was extracted. In deuterium, the beam profile is more centered than in hydrogen and it shows a better homogeneity. In hydrogen the beam is shifted strongly upwards with the result that the measurement range of the five BES lines of sight is not sufficient for determining the position of the maximum beam intensity.

The fact that this result is in general agreement with the plasma density profile shown in figure 18(a) is the result of a complex interplay of different physical effects. Taking into account only the production of the negative ions, the beam structure should depend mainly on the homogeneity of the atomic flux toward the PG (surface conversion of hydrogen atoms is the dominant process for negative ion production at the PG surface [43]). However, the plasma homogeneity close to the PG plays additionally a role, since positive ions are needed for the space charge limited transport of surface produced negative ions toward the extraction apertures [44]. Additionally, vertical deflections of the extracted beam are caused by the Lorentz force, mainly due to the fringe field of the magnetic filter field in the accelerator. The impact of the Lorentz force on particle trajectories is mass dependent and thus different for hydrogen and deuterium. A full description of the interplay of these physical effects needs to be based on model calculations, ideally taking into account both, the plasma and the beam. First

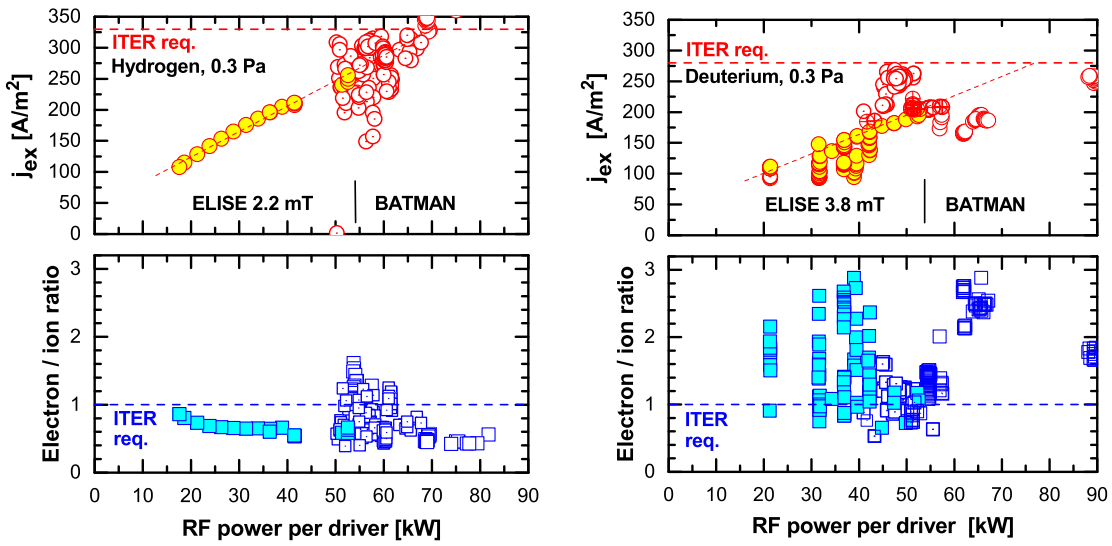

Figure 20. Comparison of the source performance at BATMAN (open symbols) and ELISE (closed symbols) in (left) hydrogen and (right) deuterium discharges at a pressure of 0.3 Pa and extraction voltages <9.5 kV.

steps of such a full description have been done using the 2D fluid code [40], the beam code BBC-NI [10] and additionally simple trajectory tracking codes.

5. Size scaling

The experience and results gained at the test facilities allow a size scaling study from the prototype source towards the ITER relevant size at ELISE, in which operational issues, physical aspects and the source performance are addressed.

5.1. Low pressure operation

In all sources, low source pressure operation with 0.3 Pa filling pressure and below is possible: 0.1 Pa was demonstrated at BATMAN [7], 0.2 Pa at ELISE [45]. However, filter field studies at the prototype source at BATMAN revealed that plasma sustainment became more difficult the closer the magnetic frame is located to the driver [30]. For example, when the magnet frame was shifted to the middle of the expansion region (increasing the magnetic field strength inside the driver), stable plasma operation was possible only for pressures at or above 0.4 Pa. This suggests that the penetration of the magnetic field into the driver plays a role as well as the 3D topology of the magnetic field. In standard configuration, with the inner magnets ($z = 3$ cm), operation at high RF power and low pressure showed a strong neutral depletion [11] such that also plasma sustainment became an issue. As in the large sources the gas flow is much higher less neutral depletion can be expected.

5.2. Short and long pulse operation

In short pulse operation, the ITER parameters with respect to negative ion current density and the amount of co-extracted electrons at 0.3 Pa have been demonstrated in the prototype source at BATMAN (4 s beams) [7], in both hydrogen and deuterium. At ELISE the first caesiation has been done in short pulses [10] and at reduced RF power levels. Figure 20 compares the source performance at BATMAN with the one at ELISE as a function of the RF power per driver. ELISE was operated with 20 s plasma including 9.5 s beams. For better comparison only data points with extraction voltages between 8.5 and 9.5 kV are plotted, which means the best results achieved at BATMAN are not included as they have been obtained at higher voltages (up to 11 kV). As shown, operation in hydrogen with a low co-extracted electron current is not an issue, neither in BATMAN nor in ELISE. The current densities of negative ions show a comparable RF efficiency in the large source as in the prototype source. From these quite encouraging results extrapolations of the measured ELISE data to the ITER value (horizontal line) are performed: a required RF power of about 70–80 kW per driver can be expected for the large source which is less than envisaged for the ITER NBI source.

Extension of the pulse length is often limited by the amount of the co-extracted electrons, in particular in deuterium operation. Being the minority in the ion–ion plasma close to the extraction the temporal and spatial behavior of the electrons is much more sensitive on the caesium dynamics. The latter is influenced by the evaporation rate and to some extent by the position, the distribution and deterioration of the caesium in the

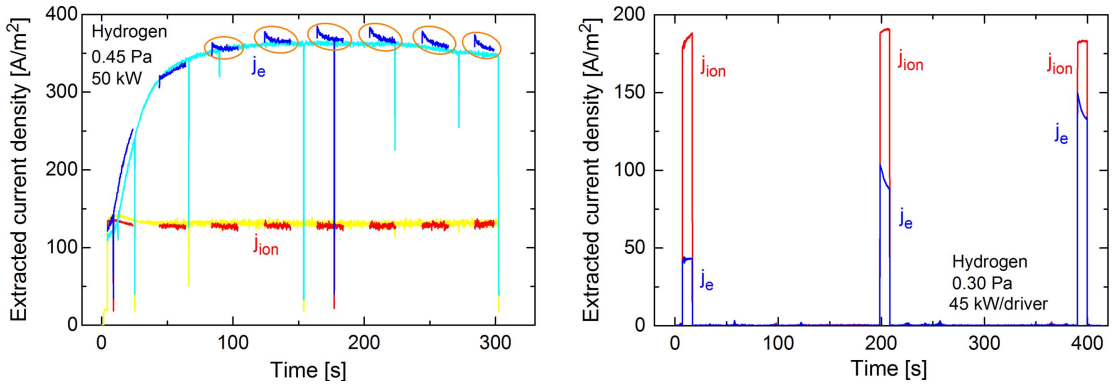

Figure 21. Left: pulsed versus continuous extraction in consecutive pulses at the MANITU test facility. Right: pulsed extraction at the test facility ELISE.

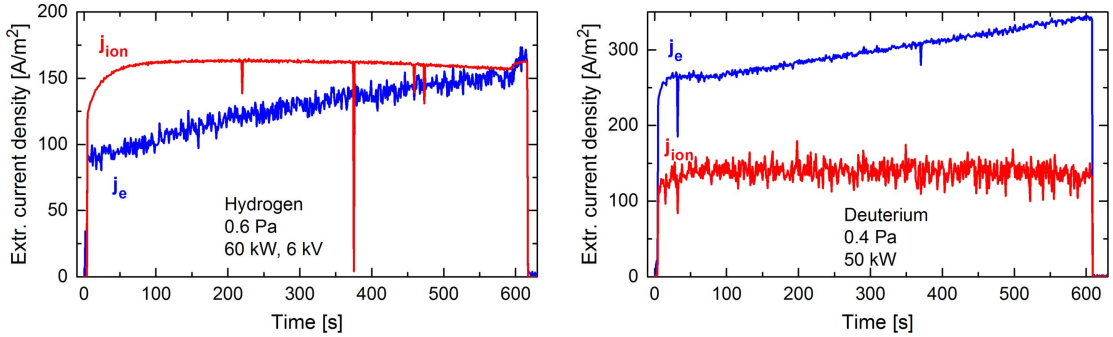

Figure 22. Extracted current densities of long pulses at the MANITU test facility in hydrogen (left) and deuterium operation (right). Beside the pressure, the power per driver and the extraction voltage are given.

vacuum phase, and by the redistribution and cleaning effect of the caesium layers during plasma phases [8, 10, 37].

Dedicated comparison has been performed between ELISE and the cw test facility MANITU [46] in order to see if cw plasma pulses combined with cw extraction (MANITU) or pulsed extraction (ELISE) led to a difference on the extracted currents. Previous experiments at MANITU showed that no difference exists for the negative ion current. However, the electrons are again much more sensitive. This can be seen in figure 21 in which two consecutive MANITU pulses are shown. Clearly, the temporal behavior of the electrons in the beam blips is different compared to cw extraction but not so pronounced as for the beam blips at ELISE shown as well in figure 21. The strong dynamics of the extracted electrons is assigned to back-streaming positive ions, created in the accelerator system, impinging on the back plate of the ion source at which caesium is cumulated and sputtered by these particles. Consequently caesium is released and redistributed in the source. This is confirmed by the time trace of the caesium emission signal (852 nm line of neutral caesium observed via a LOS parallel to the PG at 2 cm distance) showing a pronounced increase during extraction [16]. Compared to ELISE the percentage of the area of the back plate hit by the back-streaming ions is much lower at MANITU explaining the less pronounced effect. Obviously, a deconditioning of the caesium takes place between the beam blips, whereas the caesium released by the back streaming ions improves the source performance. Attempts to increase the caesium evaporation rate and thus supply more caesium to the source had the disadvantage to cause either breakdowns between the grids or RF matching problems in the driver.

Figure 22 shows the typical long pulse behavior at the prototype test facility MANITU for hydrogen and deuterium. A very good stability of the extracted ion currents is observed, whereas the co-extracted electrons increase steadily during the extraction. Similar results are observed at ELISE (see figure 15(b)). In general, this increase is more pronounced in deuterium which highlights again the relevance to control the co-extracted electrons in particularly for deuterium operation, independently of the source size [47].

5.3. Scaling of magnetic field topology, bias area and Cs consumption

The filter field at the large ITER-relevant sources created by a current through the plasma grid forms a 3D magnetic field pattern which is completely different from that of prototype source where it is generated by permanent magnets (see section 2.3). The adjustment of the PG current allows for changing the magnetic field strength without changing the 3D topology—with the exception, that the fixed field from the electron deflection magnets dominates the total magnetic field in vicinity to the PG. As already demonstrated at RADI, the plasma emission in the ELISE drivers increases with increasing field strength due the hampered plasma flow out of the driver whereas it decreases close to the plasma grid because of reduction of the plasma transport across the magnetic filter [30]. At about 0.6 kA PG current (about 0.6 mT at the PG centre), the electron temperature is already reduced to the desired value of 1 eV and the electron density is reduced as well. For the prototype source only values for the field strength of about 7 mT at different distances from the PG (3 cm for the internal magnets and 9 cm for the magnet frame) and without filter field are available resulting in temperatures in front of the PG of $\leqslant$1 eV and 4–5 eV, respectively. In view of the ITER source for which 5 kA of PG current will be available one can conclude that the filter field topology as well as the strength is sufficient to achieve the desired cooling effect needed for reducing the destruction of negative ions by electrons in front of the PG. However, for the sufficient electron suppression a higher filter field is required.

The influence of the extraction voltage and the interplay with the bias voltage applied to the plasma grid needs to be clarified as well. In contrast to the prototype source, the plasma drift is much less pronounced at ELISE. OES results imply that the plasma in front of the grid is vertically symmetric; using six horizontal LOS the intensity of Balmer lines varies less than 40% [47]. Obviously, the magnetic filter field topology together with the modular concept of having four drivers to generate the plasma with an overlapping of the particles emerging from each driver in the large expansion chamber leads to an homogeneous illumination of the 0.9 $\times$ 1 m^2 PG area by the cold plasma. Although first modeling results for these large sources are available [48], further modeling efforts are highly desired to understand the effects in more detail. Nevertheless, as the ITER source represents a doubling of the ELISE source in vertical direction a good plasma illumination of the extraction area can be expected.

The combination of both, the magnetic filter field and the PG bias, are used to suppress the amount of co-electrons to a tolerable amount without decreasing the current of negative ions [7]. The bias applied between the plasma grid and the bias plate changes the plasma sheath and hence the electron fluxes to the extraction apertures. In order to control the fluxes the bias current is a better control parameter than the bias voltage that needs to be adjusted according to changes in the plasma potential caused, for example, by pressure changes or caesium seeding [46]. The dependence of the ion current and co-extracted electron current on the bias current is very similar for the two sources taking into account that the bias current scales with the area of the bias plate (factor four higher at ELISE): the negative ions are almost independent until they start to decrease whereas the amount of co-extracted electrons shows an exponential decay until they saturate [47]. For both, an optimal point for operation is given: having almost the same ion current but with almost maximum achievable suppression of co-extracted electrons. No remarkable difference in the bias voltages (typically around 20 V) is obtained for the two sources. However, a slight difference of the bias voltage is measured for the plasma phase compared to the beam blips: applying the extraction voltage increases the bias voltage at the prototype source, while it decreases at ELISE. This indicates differences in the potential structure close to the grid which might be related to the different geometry of the bias plate at ELISE surrounding the beamlet groups as well. Here plasma potential measurements might give more insight; first measurements at ELISE are underway.

The dependence of the extracted currents on the magnetic filter field strength at the plasma grid is shown in figure 23 for both the prototype source and the ELISE source. Dedicated experiments at the prototype source revealed that a certain magnetic field at the PG is beneficial for the amount of extracted negative ions because they are bent back by the field to the apertures [5]. With increasing field strength at the PG the extracted negative ion current density decreases, resulting in the parabolic behavior sketched in figure 23. The higher the field the better the co-extracted electrons are suppressed, however revealing also a lower limit. Here the interplay with the bias current is very important and the best operation point needs to be identified individually. At ELISE similar trends are observed (figure 23). External magnets in weakening as well as in strengthening configuration have been added. Weakening the I_{PG} field by the external magnets results in much higher electron currents but strengthening the I_{PG} field results in a further reduction without affecting too much the ion currents. As demonstrated in section 4.1, the external magnets additionally can stabilize the co-extracted electron current during pulses (see figure 16). In fact, due to the large distance between the magnets (>1 m), the change of the magnetic field in the center of the plasma grid is almost negligible, but the 3D-topology changes in particular at the side walls. The comparison of deuterium with hydrogen shown in figure 23 for ELISE underlines the importance to have an adjustable filter field strength for source operation: for deuterium a stronger filter field is needed (see section 4) but the dependence on the additional magnets is similar which confirms the relevance of

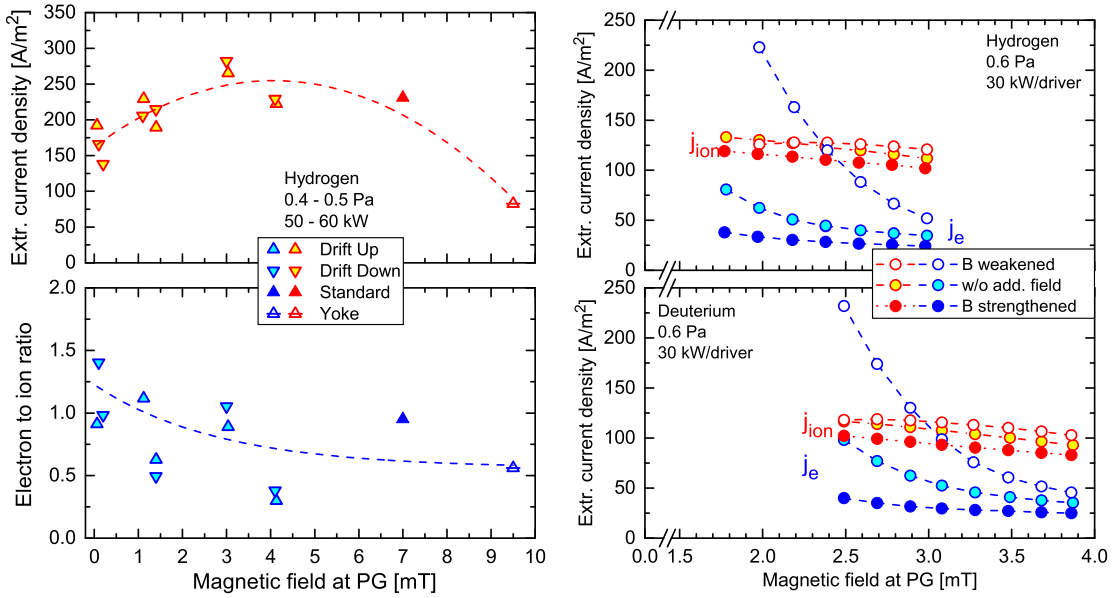

Figure 23. Left: performance of the prototype source in hydrogen using different magnetic configurations [5]. The dotted lines represent a parabolic fit (ions) and a fit with an exponential decay (electron to ion ratio). Right: performance of the ELISE source in hydrogen and in deuterium for varying magnetic field adjusted by the PG current at different configurations of attached magnets [19].

the 3D-topolgy for electron suppression. Consequently, a flexibly adjustable PG current and thus filter field strength is highly advisable also for ITER [49].

Concerning the caesium consumption typical evaporation rates of 5–10 mg h^{-1} could be estimated at the prototype source using the IPP caesium oven equipped with three Cs ampullas with 1 g Cs each as reservoir, which can be cracked individually [7]. The change to an oven which is equipped with a surface ionization detector [50], different nozzle geometry, a valve to prevent degradation of the pure caesium in the reservoir by impurities in the background gas and a well-elaborated temperature control allowed for better control and precise adjustment of the caesium evaporation. First estimates result in a factor two to three reduced evaporation rates. At the ELISE source two ovens of this kind are mounted, one at each side wall, with approximately similar total evaporation rate as in the prototype source [47]. This is positively surprising as the source is significantly larger (230 l compared to 47 l). Although the size scaling parameter for the Cs consumption is not identified yet, the recent ELISE results indicate a lower Cs consumption. This observation is very beneficial for the ITER source as caesium maintenance is one of the major issues limiting the source availability. For both sources higher caesium evaporation rates are needed for deuterium than for hydrogen (approximately a factor of two) and the conditioning is also much harder in deuterium.

Although some insights have been gained already in the complex caesium dynamics (temporally and spatially), e.g. the beneficial role of having the temperature of the source at or well above 35 °C and the grid between 125 °C and 200 °C, the relevance of building up a caesium reservoir in the vacuum phases for the next plasma pulse, etc, the caesium conditioning procedure of this large ion source is still not optimized. The experimental efforts are supported by a 3D trajectory code capable of modeling the caesium flow from the oven, the caesium transport and its redistribution in vacuum and plasma phases [51]. A large part of the required input parameters (sticking coefficient of caesium as a function of temperature, impurities in the background gas in vacuum, duration of plasma interaction) were not available in literature and are thus taken from measurements in lab scale experiments operating at ion source relevant parameters [52]. The code has been benchmarked against experimental results of the prototype source revealing also that the position of the oven is of minor relevance for the caesium distribution [53]. First results for the large source at ELISE are available revealing the strong caesium dynamics in this source with the additional effect of the caesium sputtering from the source back plate by the back-streaming positive ions [54].

5.4. Beam homogeneity

For determination of the beam uniformity data measured at the calorimeter and from BES are used at ELISE and BATMAN. For direct comparison some differences have to be taken into account: the size of the extraction area and the arrangement of the apertures, the beam divergence which is about 4°–5° at BATMAN and 1°–2° at ELISE in perveance matched conditions, the beam size and the distance to the measurement position. Because the magnet filter field has also a non-negligible horizontal component in the accelerator, the beam is vertically

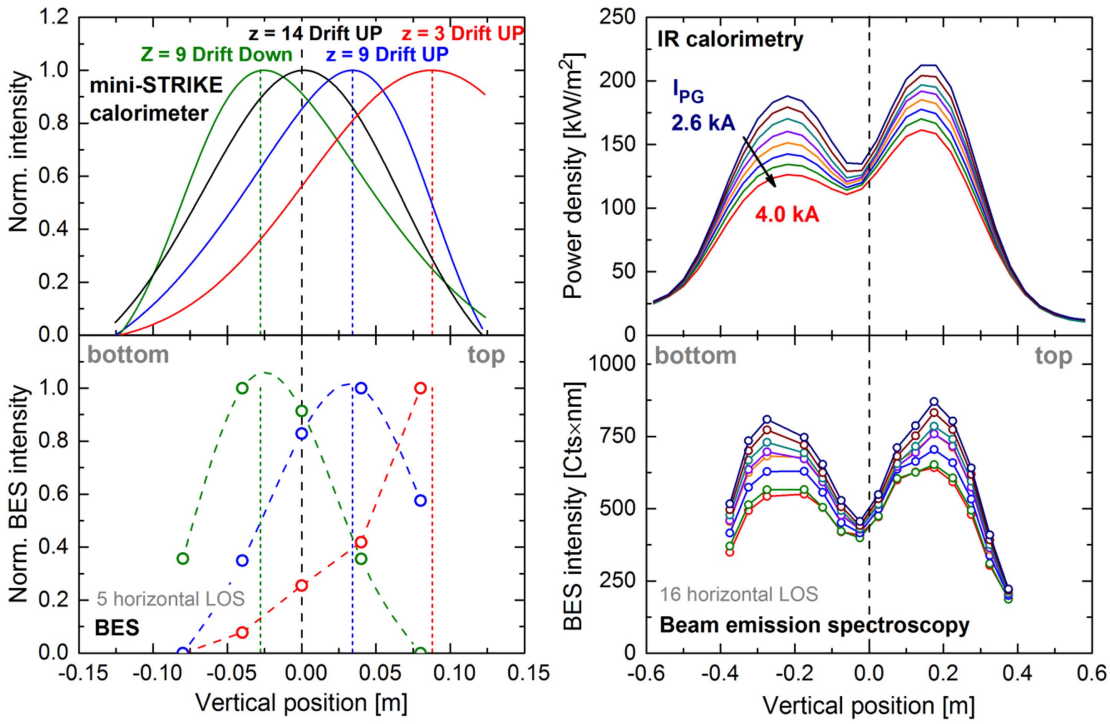

Figure 24. Vertical beam profile as measured by the mini-STRIKE test calorimeter and by BES for: (Left) different magnetic configurations of the prototype source; (Right) variation of the PG field at the test facility ELISE.

deflected, whereas the magnetic field of the deflection magnets in the extraction grid is arranged such that the polarity changes from aperture row to aperture row such that although the beam is broadened horizontally, no effective beam deflection has to be considered.

The effect of the position and polarity of the magnetic filter field on the vertical position of the beam profile is shown in figure 24 for the prototype source [55]. These measurements have been carried out using the temporarily installed test calorimeter mini-STRIKE [55] at 1 m distance from the grounded grid. At the standard magnetic configuration (internal magnets located 3 cm from the plasma grid, $z = 3$), the beam is shifted by 9 cm in upward direction corresponding to the direction of the plasma drift. The larger the distance of the magnets from the plasma grid the smaller is the beam shift. At $z = 14$ cm the magnetic field strength at the PG is about 1.4 mT only, resulting in a beam which is vertically centered. Changing the polarity in case of the $z = 9$ cm position results in a symmetrically shifted beam position. Although only five LOS compose the BES diagnostic, the shift of the beam position and the slightly asymmetric shape is visible also in the BES beam profiles. The average distance between the LOS intercepting the beam and the grounded grid is about 0.6 m.

According to the usage of permanent magnets, the magnetic field has the same horizontal direction in the source and in the accelerator at the prototype source. This is different in the large source where the field is created by the PG current resulting in a horizontal reversal of the polarity in the accelerator. Thus, the beam at ELISE is expected to be deflected downwards if the shift of beam position is solely caused by the magnetic field.

At ELISE a diagnostic calorimeter blackened by a thin layer of MoS_2 for applying infrared imaging is located in 3.5 m distance from the grounded grid whereas the BES intercepts the beam at about 2.6 m [36]. Both profile measurements reflect very well the two rows of beamlet groups with higher intensity in the upper half of the beam. With increasing magnetic field strength (PG current), this asymmetry increases slightly. As expected, the vertical position is shifted downwards by a few centimetres (between 3 and 5 cm) indicating also an increased beam shift with higher field strength. Compared to the prototype source, the shift in the beam position is less pronounced. At ELISE the direction of the PG current is chosen such that a plasma drift upward direction is expected. Thus contrary to the prototype source the influence of the plasma drift and the beam deflection on the beam position would counteract each other, if a pronounced plasma drift would be observed. As the latter is not obtained one can conclude that the beam shift is dominantly caused by the fringe field of the magnetic filter in a well caesiated source, i.e. for uniform caesiation of the plasma grid.

The detailed analysis of the Doppler-shifted H_α peaks obtained by the 20 LOS of the BES reveals an inhomogeneity of about 3% in horizontal direction and about 7% in vertical direction in a well-conditioned source and at good perveance conditions. This is very promising concerning the required beam homogeneity for the ITER source for which deviations of only 10% are allowed in order to minimize losses in the beam line.

Table 2. Comparison between the ITER requirements and achievements performed at IPP prototype and ELISE sources.

		ITER requirements		IPP prototype source (BATMAN and MANITU)				IPP (ELISE)			
Species		H^-	D^-	H^-		D^-		H^-		D^-	
Energy	keV	870	1000	23				60			
Pulse length	s	1000	3600	4.0	1000	4.0	3600	9.5	1000	9.5	3600
Extracted current density	A m^{-2}	329	286	339 (90 kW)	159 (47 kW)	319 (76 kW)	98 (43 kW)	256 (53 kW/dr.)	153 (38 kW/dr.)	176 (47 kW/dr.)	57 (21 kW/dr.)
Electron-ion-ratio		1		0.43	1.13	0.99	1.17	0.66	0.30	0.74	0.92

6. Summary

RF ion source development for negative ions is performed at IPP for 20 years at several test facilities in hydrogen as well as in deuterium, accompanied by an extensive setup of diagnostics for source and beam parameters.

The size increase from the prototype source towards the ELISE source and a different way to generate the magnetic filter field showed considerable advantages for the source performance: (i) the caesium consumption of 5–10 mg h^{-1} is not higher than in the prototype source. (ii), almost no plasma drift has been observed in the source and (iii) the drift of the beam is much less pronounced. Conditioning procedures have been elaborated which enable fast reaching of the desired level of high ion and low electron currents values, which is characterized by a change to an ion/ion plasma close to the plasma grid. In pulses of several s with the prototype source extracted current densities of 339 A m^{-2} in hydrogen and 319 A m^{-2} in deuterium have been achieved which exceed the ITER requirements (329 A m^{-2} for H^-, 286 A m^{-2} for D^-). This demonstrates the physical potential of the source concept. The ELISE source did not reach these values in short pulses, which was caused mainly by technical limitations of the RF power. Because the efficiency in both sources is almost the same, it is expected that a power of 75–80 kW per driver will be sufficient to achieve full ITER parameters. A comparison between the ITER requirements and the achievements performed at IPP prototype and ½ size ITER source is shown in table 2.

In long pulses the best results for ELISE so far were 153 A m^{-2} in hydrogen for 1000 s and 57 A m^{-2} in deuterium for one hour. The reason for the low values in deuterium operation, the increasing electron currents, has to be the key issue for future investigations. Measures to decrease the electron current like reduction of the power, higher filter field strength or higher bias potential lead simultaneously to lower ion current. A promising way seems to be the change of the filter field topology, as the experiments with additional magnets have shown. A simple way to decrease the electron current in deuterium is to raise the source pressure, in addition this would facilitate RF issues. The pressure required for ITER of 0.3 Pa is based on calculated 30% stripping losses in the accelerator. At ELISE, however, significantly lower values have been measured [56], so the 0.3 Pa limit is questionable. Commissioning and operation of the ITER size sources at the neutral beam test facilities will benefit a lot of the technical and experimental experience gained with the IPP sources.

Acknowledgments

The authors would like to thank M Barbisan, St Lishev, A Heiler, I Mario and R Maurizio for their contribution to this work and stimulating discussions.

This work has been carried out within the framework of the EUROfusion Consortium and has received funding from the Euratom research and training programme 2014–2018 under Grant Agreement No. 633053.

The work was supported by a contract from Fusion for Energy (No. F4E-2009-0PE-32-01), represented by Antonio Masiello. The opinions expressed herein are those of the authors only and do not necessarily reflect those of Fusion for Energy or the European Commission.

References

[1] Hemsworth R, Tanga A and Antoni V 2008 *Rev. Sci. Instrum.* **79** 02C109
[2] Frank P *et al* 1998 *AIP Conf. Proc.* **439** 119–22
[3] Toigo V *et al* 2015 *Nucl. Fusion* **55** 083025
[4] Kraus W *et al* 2009 *AIP Conf. Proc.* **1097** 275
[5] Franzen P *et al* 2011 *Plasma Phys. Control. Fusion* **55** 115006
[6] Kraus W *et al* 2015 *Fusion Eng. Des.* **91** 16–20
[7] Speth E 2006 *Nucl. Fusion* **46** S220
[8] Kraus W *et al* 2012 *Rev. Sci. Instrum.* **83** 02B104

[9] Franzen P et al 2007 Fusion Eng. Des. 82 07–423
[10] Franzen P et al 2015 Nucl. Fusion 55 053005
[11] Mcneely P, Wünderlich D and The NNBI-Team 2011 Plasma Sources Sci. Technol. 20 045005
[12] Heinemann B et al 2009 Fusion Eng. Des. 84 915–22
[13] Heinemann B et al 2011 Fusion Eng. Des. 86 768–71
[14] Nocentini R et al 2011 Fusion Eng. Des. 86 916–9
[15] Nocentini R et al 2009 Fusion Eng. Des. 84 2131–5
[16] Fantz U et al 2016 Rev. Sci. Instrum. 87 02B307
[17] Kraus W et al 2016 Rev. Sci. Instrum. 87 02B315
[18] Kraus W et al 2016 Rev. Sci. Instrum. 87 059901
[19] Wünderlich D et al 2016 Plasma Phys. Control. Fusion 58 125005
[20] Wünderlich D et al 2014 Plasma Sources Sci. Technol. 23 015008
[21] Fantz U et al 2013 AIP Conf. Proc. 1515 187
[22] Mcneely P et al 2009 Plasma Sources Sci. Technol. 18 014011
[23] Christ-Koch S et al 2009 Plasma Sources Sci. Technol. 18 025003
[24] Berger M et al 2009 Plasma Sources Sci. Technol. 18 025004
[25] Wimmer C, Fantz U and The NNBI-Team 2013 AIP Conf. Proc. 1515 246
[26] Fantz U and Wünderlich D 2006 New J. Phys. 8 301
[27] Fantz U et al 2006 Nucl. Fusion 46 S297
[28] Wünderlich D, Dietrich S and Fantz U 2009 J. Quant. Spectrosc. Radiat. Transfer 110 62–71
[29] Wünderlich D and Fantz U 2016 Atoms 4 26
[30] Fantz U, Schiesko L and Wünderlich D 2014 Plasma Sources Sci. Technol. 23 044002
[31] Schiesko L et al 2012 Plasma Sources Sci. Technol. 21 065007
[32] Wimmer C, Schiesko L and Fantz U 2016 Rev. Sci. Instrum. 87 02B310
[33] Barnett C F et al 1977 Internal Report 5206 (Oak Ridge, TN: Oak Ridge National Lab)
[34] Fantz U and Wimmer C 2011 Journal of Physics D 44 335202
[35] Franzen P, Wünderlich D and Fantz U 2014 Plasma Phys. Control. Fusion 56 025007
[36] Nocentini R et al 2013 Fusion Eng. Des. 88 913
[37] Fantz U, Franzen P and Wünderlich D 2012 Chem. Phys. 398 7
[38] Trevisan C S and Tennyson J 2002 Plasma Phys. Control. Fusion 44 1263
[39] Schiesko L et al 2012 Plasma Phys. Control. Fusion 54 105002
[40] Lishev S et al 2015 AIP Conf. Proc. 1655 040010
[41] Lishev S 2016 private communication
[42] Fantz U et al 2009 AIP Conf. Proc. 1097 265
[43] Wünderlich D et al 2012 Plasma Phys. Control. Fusion 54 125002
[44] Wünderlich D, Gutser R and Fantz U 2009 Plasma Sources Sci. Technol. 18 045031
[45] Franzen P et al 2013 Fusion Eng. Des. 88 3132–40
[46] Fantz U et al 2009 Nucl. Fusion 49 125007
[47] Fantz U et al 2015 AIP Conf. Proc. 1655 040001
[48] Fubiani G and Boeuf J P 2015 Plasma Sources Sci. Technol. 24 055001
[49] Chitarin G et al 2015 AIP Conf. Proc. 1655 040008
[50] Fantz U, Friedl R and Fröschle M 2012 Rev. Sci. Instrum. 83 123305
[51] Gutser R et al 2011 Plasma Phys. Control. Fusion 53 105014
[52] Friedl R and Fantz U 2014 Rev. Sci. Instrum. 85 02B109
[53] Mimo A et al 2016 Modelling of caesium dynamics in the negative ion sources at BATMAN and ELISE AIP Conf. Proc. submitted
[54] Mimo A 2016 private communication
[55] Maurizio R et al 2016 Nucl. Fusion 56 066012
[56] Fantz U et al 2016 Operation of large RF sources for H-: lessons learned at ELISE AIP Conf. Proc. submitted